

Monte-Carlo Modeling of Non-Gravitational Heating Processes in Galaxy Clusters

Mamoru SHIMIZU,¹ Tetsu KITAYAMA,² Shin SASAKI,³ and Yasushi SUTO¹

¹*Department of Physics, School of Science, The University of Tokyo, Tokyo 113-0033*

²*Department of Physics, Toho University, Funabashi, Chiba 274-8510*

³*Department of Physics, Tokyo Metropolitan University, Hachioji, Tokyo 192-0397*

mshimizu@utap.phys.s.u-tokyo.ac.jp, kitayama@ph.sci.toho-u.ac.jp,

sasaki@phys.metro-u.ac.jp, suto@phys.s.u-tokyo.ac.jp

(Received 2003 September 23; accepted 2003 October 30)

Abstract

We consider non-gravitational heating effects on galaxy clusters on the basis of the Monte-Carlo modeling of merging trees of dark matter halos combined with the thermal evolution of gas inside each halo. Under the assumption of hydrostatic equilibrium and the isothermal gas profiles, our model takes account of the metallicity evolution, metallicity-dependent cooling of gas, supernova energy feedback, and heating due to jets of radio galaxies in a consistent manner. The observed properties of galaxy clusters can be explained in models with higher non-gravitational heating efficiency than that in the conventional model. Possibilities include jet heating by the Fanaroff-Riley Type II radio galaxies, and the enhanced star formation efficiency and/or supernova energy feedback, especially at high redshifts.

Key words: cosmology: theory – dark matter – galaxies: clusters: general – X-rays: galaxies

1. Introduction

Energy feedback plays a vital role in a variety of different phenomena and scales of the universe. Supernova explosion produces an overdense shock shell in the surrounding interstellar medium which triggers the subsequent star formation. The Gunn-Peterson test in the quasar spectra has revealed that our universe was reionized at high redshifts ($z \sim 6$). The recent *WMAP* result indeed indicated that the reionization epoch may be even earlier than previously thought, $z = 17 \pm 5$ (Spergel et al. 2003). This implies that the energy feedback from first cosmological objects, or *non-gravitational heating of the universe*, was much stronger than the conventional model predictions.

Non-gravitational heating is also believed to have had a significant influence on the scales

of galaxy clusters. This is clearly illustrated by the well-known inconsistency of the observed X-ray luminosity-temperature (L_X - T) relation; $L_X \propto T^3$ (e.g., David et al. 1993; Markevitch 1998; Arnaud, Evrard 1999) against the simple self-similar prediction $L_X \propto T^2$ (Kaiser 1986). More recently Voit, Bryan (2001) suggested that the effect of cooling is important in reproducing the observed L_X - T relation (see also Wu, Xue 2002). The subsequent simulations (e.g., Muanwong et al. 2002; Kay et al. 2003; Tornatore et al. 2003), however, indicate that while the L_X - T relation can be explained by purely cooling effect, the observed hot gas fraction requires a fairly significant amount of non-gravitational heating (e.g., figure 3 of Muanwong et al. 2002 and figure 8 of Kay et al. 2003).

Physical origin of the non-gravitational heating of the intracluster medium (ICM) still remains to be understood. A plausible candidate responsible for the heating is the energy feedback by supernova explosions before and/or during the formation of galaxy clusters (Evrard, Henry 1991; Kaiser 1991). Previous authors (Cavaliere et al. 1999; Balogh et al. 1999; Pen 1999; Kravtsov, Yepes 2000; Loewenstein 2000; Wu et al. 2000; Bower et al. 2001; Brighenti, Mathews 2001), however, concluded that the excess heating energy $\sim 1\text{keV}$ per gas particle is required to account for the observed L_X - T relation. This amount of energy seems larger than the conventional model prediction of the supernova combined with the standard star formation history and the initial mass function of stars. Another candidate of the heating sources frequently discussed is active galactic nuclei (AGNs). Since the radiation from AGNs is ineffective in heating the ICM, one has to look for the kinetic energy input, from radio jets for instance, to efficiently thermalize the ICM (Wu et al. 2000). Inoue, Sasaki (2001) claimed that jets from radio galaxies can provide sufficient energy input to thermalize the ICM and explain the observed L_X - T relation on the basis of simple analytic estimates, despite several considerable uncertainties of the abundances and intrinsic properties of such radio galaxies.

In this paper, we explore extensively the consequences of non-gravitational heating processes on the observable properties of galaxy clusters. For that purpose, we follow the merging history of dark matter halos in the Monte-Carlo fashion and then trace the thermal evolution of baryonic gas inside these halos. This approach was first applied by Wu et al. (2000) in the context of the ICM heating, and our current method improves their modeling in several aspects and also approaches the problem in a complementary fashion; (i) we follow the merging tree of dark halos of mass down to $1.7 \times 10^7 M_\odot$ from $z = 30$ to $z = 0$ so as to resolve all the halos that may cool, i.e., whose virial temperature exceeds 10^4K (Shimizu et al. 2002). (ii) We simultaneously consider the supernova energy and the jets of radio galaxies as heating sources in addition to various cooling processes. Thus the thermal evolution of baryonic gas, star formation history and the metallicity evolution are solved in a consistent manner. (iii) We adopt the cooling rate which incorporates the metallicity evolution of hot gas in each halo. (iv) The overall strength of heating in our model is controlled by the two dimensionless parameters, ϵ_{SN} and ϵ_{RG} . Their values are normalized so that $\epsilon_{\text{SN}} = \epsilon_{\text{RG}} = 1$ for our canonical sets of assumptions. Nevertheless

we survey a wider range of the parameter space taking account of the fact that the nature of those sources are poorly understood, especially at high redshifts. (v) We also consider models with the enhanced star formation efficiency at high redshifts ($z > 7$) so as to look for any possible implications on the cluster L_X - T relation on the basis of the recent *WMAP* suggestion of the early reionization in the universe (Spergel et al. 2003).

The rest of the paper is organized as follows. Section 2 briefly describes our method of tracing merger trees of dark matter halos. The basic picture of the non-gravitational heating processes, supernova feedback and jets of radio galaxies, is presented in section 3. Our model to follow thermal and metallicity evolution of baryonic gas inside dark halos is shown in section 4. We derive constraints on our model parameters from the observed metallicity – temperature relation (§5) and L_X - T relation (§6). Section 7 presents further comparison between our predictions and the observed properties of galaxy clusters in X-ray band. We also briefly compare our results with that of Wu et al. (2000). We consider the enhanced star formation model at high redshift in section 8. Finally section 9 is devoted to summary and conclusions.

Throughout the paper, we adopt a conventional Λ CDM model with the following set of cosmological parameters (e.g., Spergel et al. 2003); the density parameter $\Omega_M = 0.3$, the cosmological constant $\Omega_\Lambda = 0.7$, the dimensionless Hubble constant $h_{70} \equiv H_0/(70 \text{ km s}^{-1} \text{ Mpc}^{-1}) = 1$, the baryon density parameter $\Omega_B = 0.04h_{70}^{-2}$, and the value of the mass fluctuation amplitude at $8 h^{-1} \text{ Mpc}$, $\sigma_8 = 0.84$, where $h = 0.7h_{70}$.

2. Modeling Merger Trees of Dark Matter Halos

Our approach begins with constructing realizations of merger histories of dark matter halos. Specifically we use the method (Shimizu et al. 2002) that is based on an improved version of the algorithm first proposed by Somerville, Kolatt (1999).

Consider a halo of mass M_1 located at redshift z_1 . The mass of its progenitors, M_2 , at a slightly earlier redshift $z_2 = z_1 + \Delta z(z_1)$ obeys the *mass-weighted* conditional probability function derived in the extended Press-Schechter theory (Bower 1991; Bond et al. 1991):

$$\frac{dP}{dM_2}(M_2, z_2|M_1, z_1) = \frac{\delta_{c,2} - \delta_{c,1}}{\sqrt{2\pi}(S_2 - S_1)^3} \exp\left(-\frac{(\delta_{c,2} - \delta_{c,1})^2}{2(S_2 - S_1)}\right) \left|\frac{dS_2}{dM_2}\right|, \quad (1)$$

where $\delta_{c,i} \sim 3(12\pi)^{2/3}/20D(z_i)$ (its useful approximate formula may be found in Kitayama, Suto 1996) is the critical over-density of the mass density field at a redshift of z_i , $D(z_i)$ is the linear growth rate, and $S_i \equiv \sigma^2(M_i)$ is a mass variance of the density field top-hat smoothed over the mass scale M_i . The corresponding *number-weighted* conditional probability function for M_2 is written as

$$\frac{dN}{dM_2}(M_2, z_2|M_1, z_1) = \frac{M_1}{M_2} \frac{dP}{dM_2}(M_2, z_2|M_1, z_1). \quad (2)$$

One needs an algorithm to find all the progenitors M_2^i ($i = 1 \sim N$) for M_1 which satisfy

both the mass conservation $M_1 = \sum_{i=1}^N M_2^i$ and equation (2). In reality, this cannot be solved without the knowledge of the *joint* conditional probability function for all M_2^i that is in fact not known. Therefore a variety of empirical prescriptions/tricks have been proposed so far (Kauffmann, White 1993; Somerville, Kolatt 1999; Sheth, Lemson 1999, for instance). Our algorithm basically attempts to select all the progenitors sequentially as long as M_2^i is larger than the resolution mass at z_2 , $M_{\text{res}}(z_2)$ and the total mass satisfies

$$\sum_{i=1}^N M_2^i < M_1 - \Delta M_{\text{acc}} (< M_{\text{res}}). \quad (3)$$

The value of the minimal mass $M_{\text{res}}(z_2)$ is chosen so that its virial temperature is 10^4K below which the gas cooling rate becomes substantially low. This mass resolution is important so as not to underestimate the cold gas fraction even at high redshifts. Those halos smaller than $M_{\text{res}}(z_2)$ are not separately treated in the merging tree, but they are collectively accounted for as an accretion component. This is why the expression (3) has the additional term defined as

$$\Delta M_{\text{acc}} (< M_{\text{res}}) = \int_0^{M_{\text{res}}} dM_2 M_2 \frac{dN}{dM_2} (M_2, z_2 | M_1, z_1). \quad (4)$$

We need to trace merger trees from $z=0$ to sufficiently high redshifts (we choose $z=30$) when cooling and (non-gravitational) heating of gas are virtually not yet important. This is, however, practically impossible because the number of progenitors becomes progressively larger at higher redshifts. Therefore we decided to prepare two different sets of merger trees at low redshifts ($z=0$ to $z=7$) and at high redshifts ($z=7$ to $z=30$), and trace each halo of the former at $z=7$ by using the tree of its statistical counterpart of the latter. The detail of this procedure is described in the Appendix.

First we construct a merging tree realization starting at $z=0$ back to $z=7$. Then at $z=7$, we compute masses of all the existing halos, $M_{\text{halo},i}(z=7)$, and begin to trace their history down to $z=0$. For each halo at the later timestep $z(<7)$, we search for a halo whose mass $M_{\text{halo}}(z)$ first exceeds twice the mass of its most massive progenitor at $z=7$. If this is the case, the halo is assigned its formation epoch as $z_f = z$. This procedure is repeated for all halos at any timestep with respect to the mass of the most massive progenitor at its formation epoch. In this way, we assign the sequence of formation epochs for all halos along the merging tree realization down to $z=0$.

At its formation epoch, each halo in the merger tree is assumed to obey the density profile of dark matter:

$$\rho_{\text{halo}}(r; M) = \begin{cases} \frac{\bar{\rho}(z) \delta_c(M)}{(r/r_s)(1+r/r_s)^2} & r < r_{\text{vir}} \\ 0 & r > r_{\text{vir}}, \end{cases} \quad (5)$$

where $\bar{\rho}(z) \equiv \Omega_M \rho_{c0} (1+z)^3$ is the mean density of the universe at z , ρ_{c0} is the present critical density, $\delta_c(M)$ is the characteristic density excess, and $r_s(M)$ indicates the scale radius of the halo (Navarro et al. 1996). The virial radius r_{vir} is defined according to the spherical collapse

model as

$$r_{\text{vir}}(M) \equiv \left(\frac{3M}{4\pi\bar{\rho}\Delta_{\text{nl}}} \right)^{1/3}, \quad (6)$$

and the approximation for the critical overdensity $\Delta_{\text{nl}} = \Delta_{\text{nl}}(\Omega_{\text{M}}, \Omega_{\Lambda})$ can be found in Kitayama, Suto (1996). The two parameters r_{s} and r_{vir} are related in terms of the concentration parameter:

$$c(M, z) \equiv \frac{r_{\text{vir}}(M, z)}{r_{\text{s}}(M, z)} = \frac{8.0}{1+z} \left(\frac{M}{1.4 \times 10^{14} h_{70}^{-1} M_{\odot}} \right)^{-0.13}, \quad (7)$$

where the second equality implies its empirical fitting function (Bullock et al. 2001; Oguri et al. 2001; Shimizu et al. 2003). Finally we impose the condition that the total mass inside r_{vir} is equal to M_{vir} which relates δ_{c} to c as

$$\delta_{\text{c}} = \frac{\Delta_{\text{nl}}}{3} \frac{c^3}{\ln(1+c) - c/(1+c)}. \quad (8)$$

We assume that the above profile for each halo does not change until the next formation epoch for the corresponding descendant halo. At the next formation epoch, the halo profile according to equation (5) is rebuilt with the mass at that epoch.

3. Physical Models for Non-Gravitational Heating

In this paper, we focus on two physical models for non-gravitational heating of ICM, supernova energy feedback and thermalization of jets of radio galaxies. Their basic pictures are briefly described here.

3.1. Energy feedback from supernovae

To roughly estimate the order of the available energy from supernovae, consider the following qualitative picture. If a halo with baryonic gas mass of M_{gas} cools and forms stars of mass $\Delta M_{*} \equiv f_{*} M_{\text{gas}}$, the extra heating energy is estimated as $\eta_{\text{SN}} f_{*} M_{\text{gas}} \overline{E_{\text{K}}}$, where η_{SN} is the number of supernova events per unit mass of stars and E_{K} is a typical supernova kinetic energy. The value of η_{SN} may be computed from the adopted stellar IMF (initial mass function). In the case of the Salpeter IMF $dN/d\ln M \propto M^{-x}$ with $x = 1.35$ over $0.1 M_{\odot} < M < 125 M_{\odot}$, one obtains

$$\eta_{\text{SN}} = \frac{\int_{8M_{\odot}}^{125M_{\odot}} \frac{dN}{dM} dM}{\int_{0.1M_{\odot}}^{125M_{\odot}} M \frac{dN}{dM} dM} \approx 0.007 M_{\odot}^{-1}, \quad (9)$$

if only Type II supernovae (corresponding to stars with $M > 8 M_{\odot}$) are considered as the heating source. We adopt $\overline{E_{\text{K}}} = 10^{51} \text{erg}$. Then the extra heating energy per gas particle is

$$\frac{\Delta E_{\text{SN}}}{N_{\text{gas}}} \approx \epsilon_{\text{SN}} \frac{\eta_{\text{SN}} \Delta M_{*} \overline{E_{\text{K}}}}{M_{\text{gas}}/m_{\text{p}}} = \epsilon_{\text{SN}} \eta_{\text{SN}} f_{*} m_{\text{p}} \overline{E_{\text{K}}}$$

$$\approx 3\epsilon_{\text{SN}} f_* \left(\frac{\eta_{\text{SN}}}{0.007 M_\odot^{-1}} \right) \left(\frac{\overline{E_K}}{10^{51} \text{erg}} \right) \text{keV/particle}, \quad (10)$$

where m_p is the proton mass. This is approximately the amount of energy that is required to account for the L_X - T relation of clusters as discussed in the previous literature, depending on the specific values of f_* , η_{SN} , $\overline{E_K}$, and ϵ_{SN} .

Admittedly the estimates of these values are fairly uncertain. Recent studies of the IMF (Kroupa 2001, 2002) indicate that the x of the IMF is about 1.3 for $M > 0.5 M_\odot$ and 0.3 for $0.08 M_\odot < M < 0.5 M_\odot$. In this case, $\eta_{\text{SN}} = 0.013 M_\odot^{-1}$, a factor of two larger than the above value. Furthermore the IMF is likely to be time-dependent, and η_{SN} (and/or the star formation efficiency f_*) may be significantly larger at high redshifts given the *WMAP* implication for the early cosmic reionization. Also the value of $\overline{E_K}$ may have a large scatter and the efficiency of the energy to thermalize the ICM is not clear. Thus our strategy is to adopt the fiducial values of those parameters for definiteness, and represent all the uncertainty by the overall amplitude parameter ϵ_{SN} . Our fiducial set of model parameters corresponds to $\epsilon_{\text{SN}} = 1$, but we explore a broad range $0 < \epsilon_{\text{SN}} < 10$ to reflect the uncertainty discussed above.

3.2. Jets of radio galaxies

The other important heating source that we consider in this paper is the energy input by AGNs. Since the radiation from AGNs are very inefficient in thermalizing the ICM, we consider a population of AGNs which have powerful jets, Type II of the Fanaroff-Riley radio galaxies (FR II); Type I of the FR galaxies is known to have less powerful jets and we neglect the contribution of the latter for simplicity (Enßlin et al. 1997; Valageas, Silk 1999; Enßlin, Kaiser 2000; Wu et al. 2000; Inoue, Sasaki 2001; Nath, Roychowdhury 2002).

To proceed further we need the luminosity function of the FR II radio galaxies. Willott et al. (2001) proposed three different evolution models. Specifically we adopt the intermediate evolution model (model C) which consists of two terms for low-luminosity and high-luminosity radio source populations:

$$\frac{dn_{\text{RG}}(L_{151}, z)}{d\log_{10} L_{151}} = \frac{dn_{\text{RG,L}}}{d\log_{10} L_{151}} + \frac{dn_{\text{RG,H}}}{d\log_{10} L_{151}}, \quad (11)$$

where L_{151} is luminosity of radio galaxies observed at 151MHz. The two terms are assumed to have the following forms:

$$\frac{dn_{\text{RG,L}}}{d\log_{10} L_{151}} = n_{l0} \left(\frac{L_{151}}{L_{l*}} \right)^{-\alpha_l} \exp \left(-\frac{L_{151}}{L_{l*}} \right) \times \begin{cases} (1+z)^{k_1} & z < z_{l0} \\ (1+z_{l0})^{k_1} & z \geq z_{l0}, \end{cases} \quad (12)$$

and

$$\frac{dn_{\text{RG,H}}}{d\log_{10} L_{151}} = n_{h0} \left(\frac{L_{151}}{L_{h*}} \right)^{-\alpha_h} \exp \left(-\frac{L_{151}}{L_{h*}} \right) \times \begin{cases} \exp \left[-\frac{1}{2} \left(\frac{z - z_{h0}}{z_{h1}} \right)^2 \right] & z < z_{h0} \\ \exp \left[-\frac{1}{2} \left(\frac{z - z_{h0}}{z_{h2}} \right)^2 \right] & z \geq z_{h0}. \end{cases} \quad (13)$$

The original values of the parameters in the above equations are derived for $\Omega_M = 0$, $\Omega_\Lambda = 0$ and $H_0 = 50 \text{ km s}^{-1} \text{ Mpc}^{-1}$ (Willott et al. 2001) which are summarized in table 1. We convert their luminosity function to that relevant for our cosmological model ($\Omega_M = 0.3$, $\Omega_\Lambda = 0.7$ and $h_{70} = 1$) using equation (14) in Willott et al. (2001).

Table 1. The values of the parameters for luminosity function of radio galaxies.

$n_{l0}/h_{70}^3 \text{ Mpc}^{-3}$	α_l	$L_{l*}/h_{70}^{-2} \text{ W Hz}^{-1} \text{ sr}^{-1}$	z_{l0}	k_l	
8.23×10^{-8}	0.586	1.54×10^{26}	0.710	3.48	
$n_{h0}/h_{70}^3 \text{ Mpc}^{-3}$	α_h	$L_{h*}/h_{70}^{-2} \text{ W Hz}^{-1} \text{ sr}^{-1}$	z_{h0}	z_{h1}	z_{h2}
4.80×10^{-7}	2.42	1.25×10^{27}	2.03	0.568	0.956

It still remains to find the average relation between the radio luminosity L_{151} and the kinetic power in jet L_j of the population of radio galaxies. On the basis of a physical model combined with observational constraints of hot spot advance speeds and spectral ages for FR II radio galaxies, Willott et al. (1999) derived

$$L_j = 1.5 \times 10^{45} f_j \left(\frac{L_{151}}{5.1 \times 10^{27} h_{70}^{-2} \text{ W Hz}^{-1} \text{ sr}^{-1}} \right)^{6/7} h_{70}^{-2} \text{ erg s}^{-1}, \quad (14)$$

where f_j is a fudge factor reflecting uncertainties of the physical condition inside the jet lobes (e.g., departures from equipartition, proton and low-energy electron content). Willott et al. (1999) suggested $f_j = 1 \sim 20$, and we use $f_j = 10$ following other independent studies (e.g., Leahy, Gizani 2001; Hardcastle, Worrall 2000; Blundell, Rawlings 2000; see also §3.2 of Inoue, Sasaki 2001). Moreover Inoue, Sasaki (2001) showed that equation (14) underpredicts the observed jet luminosities (Rawlings 1992) by an order of magnitude (see figure 1 of Inoue, Sasaki 2001).

Therefore our model adopts the relation of

$$L_j = 1.5 \times 10^{47} \left(\frac{L_{151}}{5.1 \times 10^{27} h_{70}^{-2} \text{ W Hz}^{-1} \text{ sr}^{-1}} \right)^{6/7} h_{70}^{-2} \text{ erg s}^{-1}. \quad (15)$$

In order to obtain the total jet energy from L_j , one needs a typical value of the lifetime of jets, t_{life} . Using a simple model of Falle (1991) combined with the data of 7C Redshift Survey and 3CRR sample, Willott et al. (1999) derived a constraint $2 \times 10^6 \text{ yr} \lesssim t_{\text{life}} \lesssim 10^8 \text{ yr}$ for $L_{151} \gtrsim 5.1 \times 10^{27} h_{70}^{-2} \text{ W Hz}^{-1} \text{ sr}^{-1}$. So we adopt $t_{\text{life}} = 10^7 \text{ yr}$ for all radio galaxies just for simplicity and definiteness. The above set of parameters yields a value of the extra heating energy per gas particle for a halo of gas mass M_{gas} hosting one FR II radio galaxy:

$$\begin{aligned} \frac{\Delta E_{\text{RG}}}{N_{\text{gas}}} &= \epsilon_{\text{RG}} \frac{L_j t_{\text{life}}}{M_{\text{gas}}/m_p} \\ &\approx 2\epsilon_{\text{RG}} \left(\frac{L_j}{1.5 \times 10^{47} \text{ erg/s}} \right) \left(\frac{t_{\text{life}}}{10^7 \text{ year}} \right) \left(\frac{10^{13} M_\odot}{M_{\text{gas}}} \right) \text{ keV/particle}. \end{aligned} \quad (16)$$

Inoue, Sasaki (2001) suggest that the efficiency of the thermalization of the jet kinetic energy may be $0.25 \sim 0.4$ if the work done by jets stops when the pressures inside and outside of jets are equal to each other. Again we introduce a fudge factor, ϵ_{RG} , to represent overall uncertainty in our fiducial set of physical parameters.

Equation (16) indicates that the FR II radio galaxies may be another potential candidate for the non-gravitational heating sources of ICM. We emphasize, however, the significant difference between the supernova energy feedback and the jet heating; while the former is ubiquitous and always accompanies the star formation, the latter is a relatively rare event. The number density of the FR II radio galaxies, $n_{\text{RG}}(z)$, is $\sim 2 \times 10^{-7} h_{70}^3 \text{Mpc}^{-3}$ at $z=0$ [c.f., equation (23)]. Thus one FR II per dark matter mass of $\bar{\rho}(0)/\bar{n}_{\text{RG}}(z=0) \sim 2 \times 10^{17} h_{70}^{-1} M_{\odot}$. Over the cosmic age of 10^{10}yr , we may have $10^{10} \text{yr}/t_{\text{life}}$ generations of radio galaxies, and thus we expect a dark halo of mass $\sim 2 \times 10^{14} (10^7 \text{yr}/t_{\text{life}}) h_{70}^{-1} M_{\odot}$ hosts one FR II radio galaxy on average. This implies that a typical rich cluster has been heated by the jet only for a short duration in the past. Thus the jet heating needs to be simulated in a stochastic fashion as in our Monte-Carlo approach. In contrast, the amount of the supernova feedback is basically proportional to the halo mass, and thus can be taken into account statistically. In other words, the jet heating may induce significant variations in the observed L_X - T relation of galaxy clusters, and even produce a population of outliers from the mean relation.

4. Thermal and metallicity evolution of baryonic gas inside dark matter halos

Given the above two major scenarios for non-gravitational heating of ICM, we describe our detailed models to trace thermal and metallicity evolution of baryonic gas inside dark matter halos.

4.1. Gas cooling

We assume that the hot gas is isothermal with temperature T_{gas} and in hydrostatic equilibrium under the gravitational potential of the dark halo. Since we adopt equation (5) for the dark halo profile, the corresponding gas density profile is analytically expressed as follows (Suto et al. 1998):

$$\rho_{\text{hot}}(r) = \rho_{\text{hot},0} \exp[-Bf(r/r_s)], \quad (17)$$

where

$$B = \frac{2c}{\ln(1+c) - c/(1+c)} \frac{T_{\text{vir}}}{T_{\text{gas}}}, \quad (18)$$

$$f(x) = 1 - \frac{1}{x} \ln(1+x). \quad (19)$$

We define the virial temperature T_{vir} as

$$k_B T_{\text{vir}} = \frac{1}{2} \mu m_p \frac{GM_{\text{vir}}}{r_{\text{vir}}}, \quad (20)$$

where G is the gravitational constant, μm_p is a mean molecular weight ($\mu \simeq 0.6$), k_B is the Boltzmann constant. The amplitude $\rho_{\text{hot},0}$ is computed so as to reproduce the total hot gas mass in each halo when integrating equation (17) within $r = r_{\text{vir}}$.

Once the gas profile is specified, we compute the cooling radius r_{cool} within which the gas cools at each redshift z or the cosmic time $t(z)$. The gas cooling time-scale at a radius r is given by

$$t_{\text{cool}}(r) = \frac{3}{2} \frac{\rho_{\text{hot}}(r)}{\mu m_p} \frac{k_B T_{\text{gas}}}{\Lambda(T_{\text{gas}}, Z) [n_{\text{H}}(r)]^2}, \quad (21)$$

where $\Lambda(T_{\text{gas}}, Z)$ is the cooling rate of gas with temperature T_{gas} and metallicity Z , and $n_{\text{H}}(r)$ is the number density of hydrogen (including both neutral and ionized). We compute the evolution of Z for each halo simultaneously, and apply the relevant cooling rate $\Lambda(T_{\text{gas}}, Z)$ by using tables in Sutherland, Dopita (1993). For physically reasonable profiles, equation (21) is a monotonically increasing function of r , and r_{cool} is computed from the condition:

$$t_{\text{cool}}(r_{\text{cool}}) = \tau_{\text{cool}}(z) \equiv t(z) - t(z_{\text{f}}(M_{\text{f}})). \quad (22)$$

While $\tau_{\text{cool}}(z)$ in the above equation *conceptually* denotes the elapse time that gas in each halo can spend for cooling, its exact definition is fairly uncertain. In the second equality, we adopted the definition of Shimizu et al. (2002) based on the following simple picture; when a halo of mass M_{f} *forms* at the formation redshift z_{f} , its hot gas is supposed to reach the profile [equation (17)] instantaneously. This defines the origin of the cooling time for the halo, and τ_{cool} is set to the elapsed cosmic time since z_{f} . In the subsequent timesteps, we neglect the change in the hot gas profile, gas temperature, and metallicity, even if the halo mass M grows due to mergers. At each formation epoch of the host halo, its hot gas profile is reset to the profile [equation (17)] corresponding to the new mass and temperature, and the origin of τ_{cool} is replaced by that at the new formation epoch.

We apply this procedure for all halos, and the cold gas in each progenitor halo is simply accumulated according to the merger trees. For halos that do not have any direct progenitor at higher redshifts, we assume that they consist of hot gas only with no excess energy and no metals, and set their gas temperature as the virial temperature of the halos. The accreted gas [to represent the gas components below our mass resolution, see equation (4)] is always assumed to join the hot gas component of the halo without excess energy or metals.

4.2. Gas heating

At the formation epoch of each halo (i.e., each mass doubling time to be more specific), we compute the increase of the cold gas mass ΔM_{cold} of the halo since the previous formation epochs of all progenitor halos.

The increased amount of the cold gas mass ΔM_{cold} is assumed to instantaneously form stars of mass $\Delta M_* = (1 - f_{\text{rh}})\Delta M_{\text{cold}}$ while the rest of it $f_{\text{rh}}\Delta M_{\text{cold}}$ is reheated by the supernova energy and returns to the hot gas of the halo. The returned hot gas carries the metals produced

by massive stars and pollutes the hot gas associated with the halo. Observationally, metal (especially, Fe) abundances of hot gas around NGC 1399, a cD galaxy in the Fornax Cluster are estimated as $1.1^{+1.3}_{-0.5} Z_{\odot}$ within 360 kpc (Ikebe et al. 1992), and $1.5\text{--}2.0 Z_{\odot}$ within 20 kpc (Buote 2002). Theoretical models of metal ejection from elliptical galaxies by galactic wind also suggests a higher than the solar abundance (e.g., David et al. 1990), independently of the mass of stars at their final stage. Therefore we assume that the metallicity of the returned hot gas, Z_{eject} , is equal to $2 Z_{\odot}$.

In addition to the supernova heating, we incorporate the energy input by radio galaxies as follows. First, we compute the number density, $n_{\text{RG}}(z)$, of the radio galaxies at z using equations (11), (12), (13), and table 1:

$$n_{\text{RG}}(z) = \int_{\log_{10} L_{151, \min}}^{\infty} \frac{dn_{\text{RG}}}{d\log_{10} L_{151}}(L_{151}, z) d\log_{10} L_{151}. \quad (23)$$

We assume that the minimum luminosity of the radio galaxies $L_{151, \min}$ is $1.6 \times 10^{25} h_{70}^{-2} \text{ W Hz}^{-1} \text{ sr}^{-1}$ at 151 MHz, which corresponds to the FR I/FR II dichotomy in the radio morphology (Bicknell 1995; Laing 1996; Fabian 2001).

Next, we compute the expected number, $\overline{N}_{\text{RG}}(M_{\text{halo}}, z)$, of the radio galaxies for a halo M_{halo} at z during each time step of the merging tree realization $\Delta t_{\text{tree}}(z)$:

$$\overline{N}_{\text{RG}}(M_{\text{halo}}, z) = \frac{M_{\text{halo}} n_{\text{RG}}(z)}{\int_{M_{\min}}^{\infty} M n_{\text{PS}}(M, z) dM} \frac{\Delta t_{\text{tree}}(z)}{t_{\text{life}}}, \quad (24)$$

where the minimum mass of halos that host radio galaxies is set as $M_{\min} = 10^{12} M_{\odot}$. In the above equation, $n_{\text{PS}}(M, z)$ is the mass function of dark halos for which we use the Press-Schechter formula for definiteness. Note that the last factor in equation (24) accounts for the number of *generations* of the radio galaxies during $\Delta t_{\text{tree}}(z)$.

Finally, we randomly assign the radio galaxies to each halo in merger trees for $z < 7$ (we ignore the jet heating for $z > 7$) according to the expected number. As in the above treatment of the gas, we sum up the number of radio galaxies at each timestep but input the corresponding jet heating only at the formation epoch of the host halo. This procedure gives rise to the stochasticity in the heating. The radio luminosity of each radio galaxy is randomly assigned according to the observed luminosity function. We denote the amount of total energy input at the formation epoch by ΔE_{RG} .

4.3. Determining the gas temperature with the non-gravitational heating

We compute the total amount of excess energy ΔE_{gas} for each halo at its formation epoch:

$$\Delta E_{\text{gas}} \equiv E_{\text{ex,prog}} + \Delta E_{\text{SN}} + \Delta E_{\text{RG}} - \Delta E_{\text{cool}}, \quad (25)$$

where $E_{\text{ex,prog}}$ is the total excess energy already stored in all the progenitor halos, ΔE_{SN} and ΔE_{RG} indicate the excess energies from supernova feedback and jets of radio galaxies since the

last formation epoch of the progenitor halos, and ΔE_{cool} is the loss of the excess energy due to radiative cooling.

The total energy loss ΔE_{cool} is calculated as $\Delta E_{\text{cool}} = \sum_i e_{\text{ex},i} \Delta M_{\text{cold},i}$, where $e_{\text{ex},i} \equiv 3k_{\text{B}}(T_{\text{gas},i} - T_{\text{vir},i})/(2\mu m_{\text{p}})$ and $\Delta M_{\text{cold},i}$ is the increase of cold gas mass since the previous formation epoch of each progenitor halo i .

The excess energy thermalizes the surrounding ICM as well as exerts work against gravity (e.g., Wu et al. 2000). If we neglect the contribution of self-gravity of the gas, we can define the total gravitational energy of the gas as follows:

$$E_{\text{grav}}(T_{\text{gas}}) = \int \rho_{\text{hot}}(r) \Phi_{\text{halo}}(r) dV, \quad (26)$$

where $\Phi_{\text{halo}}(r)$ is the gravitational potential energy of the halo and given as

$$\Phi_{\text{halo}}(r) = -4\pi G r_s^2 \delta_c \bar{\rho}(z) \left[\frac{\ln(1 + r/r_s)}{r/r_s} - \frac{1}{1+c} \right] \quad (27)$$

for the density profile of equation (5). Then the total energy of gas of temperature T_{gas} is written as the sum of the above gravitational energy and the thermal energy $E_{\text{thermal}}(T_{\text{gas}})$:

$$E_{\text{gas}}(T_{\text{gas}}) = E_{\text{grav}}(T_{\text{gas}}) + E_{\text{thermal}}(T_{\text{gas}}). \quad (28)$$

Since we assume that the hot gas in each halo is isothermal, $E_{\text{thermal}}(T_{\text{gas}})$ is simply equal to $3M_{\text{hot}}k_{\text{B}}T_{\text{gas}}/(2\mu m_{\text{p}})$, where M_{hot} is the mass of hot gas component in the halo.

Now we are in a position to determine the gas temperature with the given energy budget. In reality this is not easy as in the empirical approach that we attempt here, since we do not know the efficiency of even *gravitational* shock heating. Therefore we first adopt a conventional assumption in modeling galaxy clusters that the gravitational shock heating is sufficiently effective to keep the gas temperature T_{gas} equal to its virial temperature T_{vir} . Then we adopt that an additional assumption that the excess energy ΔE_{gas} is exclusively consumed to increase the temperature beyond T_{vir} . Thus we solve the following equation for T_{gas} given $E_{\text{gas}}(T_{\text{vir}})$ from gravitational shock heating and the excess energy due to non-gravitational heating [equation (25)]:

$$E_{\text{gas}}(T_{\text{gas}}) = E_{\text{gas}}(T_{\text{vir}}) + \Delta E_{\text{gas}}. \quad (29)$$

4.4. Diffuse gas and the metallicity evolution

With the presence of non-gravitational heating, it occasionally happens that the gas temperature becomes much higher than the virial temperature of the halo, and hydrostatic equilibrium is unrealistic. In order to take account of such cases properly, we assume that hot gas is completely ejected from the host halo if the ratio $T_{\text{gas}}/T_{\text{vir}}$ exceeds the critical ratio f_{diffuse} . The ejected gas is not bound to the halo, but assumed to exist as a *diffuse* gas component with no subsequent thermal and metallicity evolution. The diffuse component joins the bound hot gas component again when the descendent of the progenitor halo increases its halo mass so that

its virial temperature T'_{vir} exceeds $T_{\text{gas}}/f_{\text{diffuse}}$ of the diffuse gas. Then the diffuse gas returns to the hot gas carrying the total gas energy and the metals acquired at the time when it is ejected. While we use the value of $f_{\text{diffuse}} = 10$, the results at $z = 0$ are insensitive to the choice for $10 \lesssim f_{\text{diffuse}} \lesssim 100$ since the hydrostatic configuration itself [equation (17)] is very shallow and effectively approximates a profile close to the diffuse component.

Finally the mass of metals for each halo is traced according to

$$M_Z \equiv M_{Z,\text{prog}} + Z_{\text{eject}} f_{\text{rh}} \Delta M_{\text{cold}} - \sum_i Z_i \Delta M_{\text{cold},i}, \quad (30)$$

where $M_{Z,\text{prog}}$ is the total mass of metals in all the progenitors, and Z_i denotes the metallicity in each progenitor halo i . As explained in §4.2, we set $Z_{\text{eject}} = 2Z_{\odot}$.

In passing, we summarize in table 2 the parameters used in modeling thermal and metallicity evolution of gas. Our model is characterized by the three free parameters f_{rh} , ϵ_{SN} , and ϵ_{RG} , which represent the fraction of the reheated gas due to the supernova feedback, and the (dimensionless) strengths of the supernova heating and the jet heating that we explore in the subsequent sections.

Table 2. Parameters in the present model.

symbol	adopted value	physical meaning
τ_{cool}	halo mass doubling time	time for cooling gas in each host halo
η_{SN}	$0.007 M_{\odot}^{-1}$	the number of supernovae per unit mass of stars formed out of cold gas
E_{kin}	10^{51} erg	kinetic energy of supernova explosion
Z_{eject}	$2 Z_{\odot}$	metallicity of the ejected gas
L_{j}	equation (15)	kinetic luminosity of jets of an FR II radio galaxy
t_{life}	10^7 yr	life time of jets of an FR II radio galaxy
f_{diffuse}	10	a ratio to define the diffuse gas component
f_{rh}	(free)	reheated gas fraction of cold gas to ICM
$1 - f_{\text{rh}}$	—	star formation efficiency
ϵ_{SN}	(free)	efficiency of energy input by supernova feedback
ϵ_{RG}	(free)	efficiency of energy input by jets of radio galaxies

5. Constraints from the metallicity–temperature relation

In order to avoid working in the three-dimensional parameter space, we attempt to put constraints on f_{rh} from the metallicity–temperature relation of clusters. Since the metallicity is produced by the reheated gas from supernova explosion, we can neglect the effect of the radio galaxy heating ($\epsilon_{\text{RG}} = 0$) except when ϵ_{SN} is very small (< 0.5) as discussed below. We first generate many realizations of clusters at $z = 0$ over a wide range of mass systematically

changing the values of f_{rh} and ϵ_{SN} . For each cluster, we compute the gas temperature T_{gas} and the metallicity Z according to the procedure described in the last section. Also we compute its bolometric luminosity as:

$$L_{\text{bol}} = 4\pi \int_0^{r_{\text{vir}}} \Lambda(T_{\text{gas}}, Z) [n_{\text{H}}(r)]^2 r^2 dr. \quad (31)$$

From those simulated clusters, we select samples whose gas temperature T_{gas} is higher than 2.5 keV *and* whose bolometric luminosity is larger than $0.1 \overline{L}_{\text{bol}}(T_{\text{gas}})$ at its gas temperature, where $\overline{L}_{\text{bol}}(T_{\text{gas}})$ is the mean bolometric luminosity of clusters in the observational sample compiled by Ikebe et al. (2002). The lower limit on the luminosity is introduced so as to incorporate the observational flux limit approximately, but our results are insensitive the value. For that selected sample of simulated clusters (N_{sel} in total), we compute the statistics:

$$\chi_{\text{red}}^2 = \frac{1}{N_{\text{sel}}} \sum_{i=1}^{N_{\text{sel}}} \frac{[Z_{\text{model},i} - \overline{Z}_{\text{obs}}(T_{\text{model},i})]^2}{\sigma_{\text{obs},Z}^2}, \quad (32)$$

$$\overline{Z}_{\text{obs}}(T) = [0.298 - 0.005(T/\text{keV})] Z_{\odot}, \quad (33)$$

where $Z_{\text{model},i}$ and $T_{\text{model},i}$ are the metallicity and the gas temperature of i -th cluster in the sample ($i = 1 \sim N_{\text{sel}}$). The mean metallicity-temperature relation $\overline{Z}_{\text{obs}}(T)$ is fitted from the observed data of Fe abundances of Fukazawa et al. (1998). The corresponding standard deviation in the observed data is computed as

$$\sigma_{\text{obs},Z}^2 = \frac{1}{N_{\text{obs}}} \sum_{i=1}^{N_{\text{obs}}} [Z_{\text{obs},i} - \overline{Z}_{\text{obs}}(T_{\text{obs},i})]^2, \quad (34)$$

where $N_{\text{obs}} (= 40)$ is the total number of the sample of clusters in Fukazawa et al. (1998), and $Z_{\text{obs},i}$ and $T_{\text{obs},i}$ are the metallicity and the gas temperature of the i -th cluster. We obtain $\sigma_{\text{obs},Z} \approx 0.063 Z_{\odot}$.

Examples of the predicted Z - T_{gas} relation are shown in figure 1. As expected, the metallicity is mainly determined by the reheated gas fraction f_{rh} . The contours of χ_{red}^2 on the $f_{\text{rh}} - \epsilon_{\text{SN}}$ plane (for $\epsilon_{\text{RG}} = 0$) are plotted in figure 2. Note that ϵ_{SN} represents the *efficiency* of the supernova energy feedback in our model, and the supernova rate η_{SN} is assumed to be independent of the value of ϵ_{SN} . This is why our model has metallicity evolution even when $\epsilon_{\text{SN}} = 0$ as long as the hot gas cools and forms cold gas and stars. The resulting metallicity increases as f_{rh} , but decreases as ϵ_{SN} since the star formation rate is suppressed due to the stronger energy input from the supernovae. When $\epsilon_{\text{SN}} \gtrsim 3$, however, the result becomes almost insensitive to ϵ_{SN} and simply determined by the value of f_{rh} alone. In this regime, heating is so strong and the suppression of gas cooling is almost saturated. Thus the further increase of the energy feedback does not change the result.

Just for the convenience of the analyses below, we obtained an empirical fit to the $f_{\text{rh}} - \epsilon_{\text{SN}}$ relation from figure 2 which reproduces the observational metallicity-temperature relation:

$$\epsilon_{\text{SN}} \sim \tan \left[\frac{5\pi}{3} (f_{\text{rh}} - 0.2) \right] \quad (f_{\text{rh}} \lesssim 0.5). \quad (35)$$

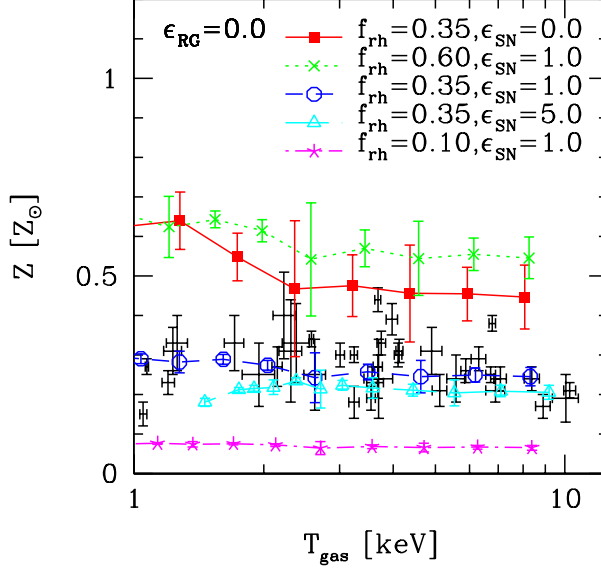


Fig. 1. Metallicity-temperature relations of clusters at $z = 0$. The dots with vertical and horizontal error-bars indicate the observational data Fukazawa et al. (1998). The other symbols with vertical error-bars represent the mean and the corresponding standard deviation from 10 realization halos sorted according to their gas temperature.

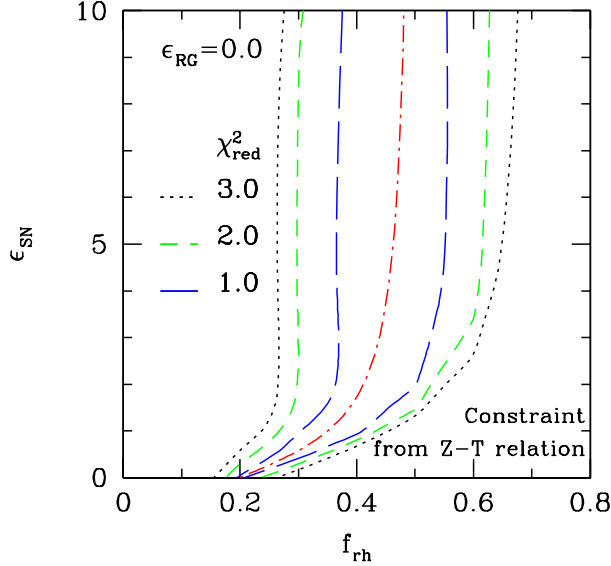


Fig. 2. Constraints on $(f_{\text{rh}}, \epsilon_{\text{SN}})$ from the observed metallicity-temperature relation by Fukazawa et al. (1998). The contours of $\chi^2_{\text{red}} = 1, 2$ and 3 are plotted. The best-fit empirical relation [equation (35)] that reproduces the observational metallicity-temperature is plotted in dot-dashed line.

It is encouraging that the resulting range, $0.2 \lesssim f_{\text{rh}} \lesssim 0.5$, is roughly consistent with other models of evolution of elliptical galaxies (David et al. 1990, 1991a, 1991b; Elbaz et al. 1995).

We also repeat the above analysis for $\epsilon_{\text{RG}} \neq 0$, and do not find significant difference as long as $\epsilon_{\text{SN}} \gtrsim 0.6$ because heating by radio galaxies is rather stochastic as noted in §3.2 and

does not affect the mean properties of clusters compared with the supernova feedback (see also figure 5 below).

6. Constraints from the luminosity–temperature relation

Let us move next to deriving constraints on the $\epsilon_{\text{SN}} - \epsilon_{\text{RG}}$ plane from the observed $L_{\text{bol}} - T_{\text{gas}}$ relation of clusters. In doing so, we fix the value of f_{rh} as a function of ϵ_{SN} so as to reproduce the metallicity – temperature relation. To be specific, we invert equation (35) and adopt

$$f_{\text{rh}} = \frac{3}{5\pi} \arctan(\epsilon_{\text{SN}}) + 0.2. \quad (36)$$

We would like to confront our simulated cluster samples at $z = 0$ with the observational data combined by Ikebe et al. (2002). The latter is a flux-limited sample of the flux limit $S_{\text{lim}} = 2 \times 10^{-11} \text{ erg s}^{-1} \text{ cm}^{-2}$ in the 0.1–2.4 keV band with spectroscopically measured temperature for $T_{\text{gas}} > 2.5 \text{ keV}$. The number of these clusters is $\tilde{N}_{\text{obs}} = 52$ in total. Since our simulated clusters are not assigned the distance, we cannot construct the corresponding flux-limited sample in reality. Thus we select those simulated clusters whose gas temperature T_{gas} is higher than 2.5 keV *and* whose bolometric luminosity is larger than $0.1 \overline{L_{\text{bol}}}(T_{\text{gas}})$ as in the previous section.

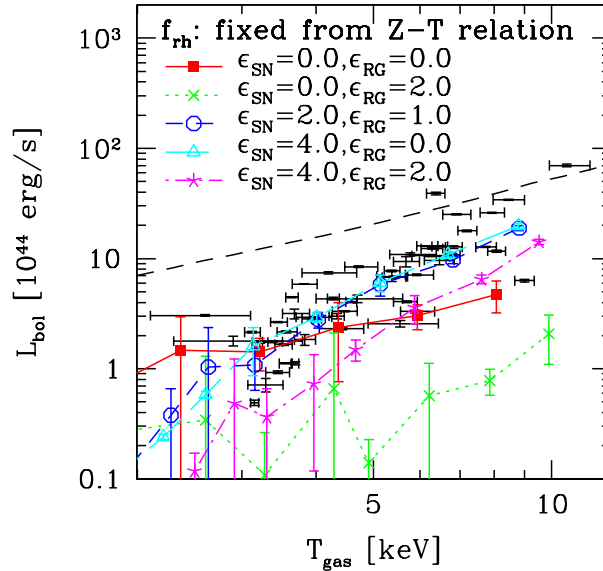


Fig. 3. Luminosity-temperature relations of clusters at $z = 0$. The dots with vertical and horizontal error-bars indicate observational data from Ikebe et al. (2002). The other symbols with vertical error-bars represent the mean and the corresponding standard deviation from 10 realization halos sorted according to their gas temperature. The dashed line indicates the ‘self-similar’ relation, in which all baryons in the halo have $T_{\text{gas}} = T_{\text{vir}}$.

For such selected samples of simulated clusters, we compute

$$\tilde{\chi}_{\text{red}}^2 = \frac{1}{N_{\text{sel}}} \sum_{i=1}^{N_{\text{sel}}} \frac{[\log_{10}(L_{\text{model},i}/10^{44} \text{ erg s}^{-1}) - \overline{F_{\text{obs,logL}}}(T_{\text{model},i})]^2}{\sigma_{\text{logL}}^2}, \quad (37)$$

$$\overline{F_{\text{obs,logL}}}(T) = -1.17 + 2.81 \log_{10}(T/\text{keV}), \quad (38)$$

where $L_{\text{model},i}$ and $T_{\text{model},i}$ are the bolometric luminosity and the gas temperature of the i -th simulated cluster ($i = 1 \sim N_{\text{sel}}$). The function $\overline{F_{\text{obs,logL}}}(T)$ is our best-fit ‘ $\log_{10} L_{\text{bol}} - \log_{10} T_{\text{gas}}$ ’ relation to the data of Ikebe et al. (2002). The corresponding standard deviation in the observed data is computed as

$$\sigma_{\text{logL}}^2 = \frac{1}{\tilde{N}_{\text{obs}}} \sum_{i=1}^{\tilde{N}_{\text{obs}}} \left[\log_{10} \left(\frac{L_{\text{obs},i}}{10^{44} \text{ erg s}^{-1}} \right) - \overline{F_{\text{obs,logL}}}(T_{\text{obs},i}) \right]^2, \quad (39)$$

where $L_{\text{obs},i}$ and $T_{\text{obs},i}$ are the bolometric luminosity and the gas temperature of the i -th observed cluster ($i = 1 \sim \tilde{N}_{\text{obs}}$). We obtain $\sigma_{\text{logL}} = 0.24$.

In order to perform the fit over a wide dynamic range of the bolometric luminosities, we decided to do so in logarithmic scales instead of in linear scales. Thus the variable $\tilde{\chi}_{\text{red}}^2$ does not obey the standard χ^2 -distribution. We use the value to examine simply the degree of the goodness-of-fit between our model and the observation, and do not intend to assign any statistical significance in a strict sense.

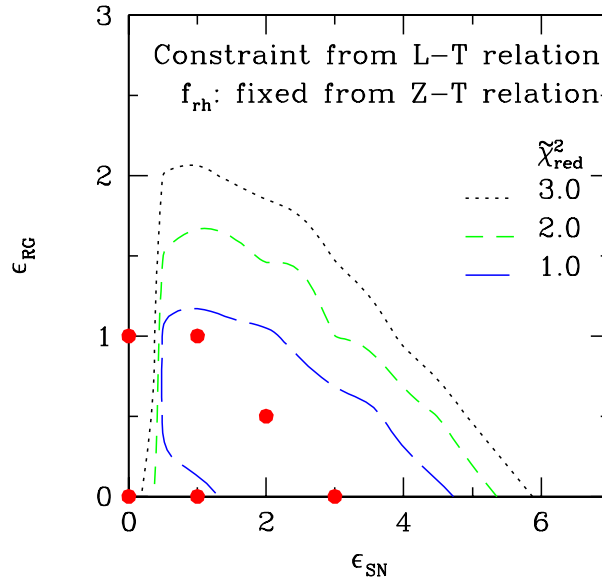


Fig. 4. Constraints on $(\epsilon_{\text{SN}}, \epsilon_{\text{RG}})$ from the observed luminosity-temperature relation by Ikebe et al. (2002). The contours of $\tilde{\chi}_{\text{red}}^2 = 1, 2$, and 3 are plotted. We fix the value of f_{rh} according to equation (36). The six filled circles indicate the parameter sets whose statistical properties are examined in detail later (§7).

Figure 3 shows examples of our model L_X – T relation against the observational data. This clearly indicates that the L_X – T relation is very sensitive to the efficiency of the non-gravitational heating processes as expected. The case of purely gravitational heating ($\epsilon_{\text{SN}} = \epsilon_{\text{RG}} = 0$; solid line with solid squares) reproduces the slope of the analytical self-similar prediction (dashed

line). Our model incorporating gas cooling, however, results in a significant fraction of cold gas in all clusters (see figure 8 below), and the amplitude is lower than the latter in this case. The change of the L_X – T relation is induced through those of the cold gas fraction and the hot gas density profile due to non-gravitational heating.

Figure 4 plots the contours of $\tilde{\chi}_{\text{red}}^2$ on $\epsilon_{\text{SN}} - \epsilon_{\text{RG}}$ plane. As is well known, the supernova feedback (or more strictly, any uniformly heating source of the ICM) is needed to account for the observed L_X – T relation. The jet of radio galaxies alone cannot provide the required degree of heating for clusters. Keeping the constraint in mind, we will examine various statistical properties of clusters in the next section. In particular we focus on the six sets of parameters, $(\epsilon_{\text{SN}}, \epsilon_{\text{RG}}) = (0.0, 0.0)$, $(0.0, 1.0)$, $(1.0, 0.0)$, $(1.0, 1.0)$, $(3.0, 0.0)$, and $(2.0, 0.5)$, plotted in figure 4. Incidentally Kay et al. (2003) conducted similar studies using cosmological hydrodynamic simulations. While we compute the SN gas temperature/entropy from the amount of the heating energy [equation (29)], they explicitly assume its temperature. Thus direct comparison with their simulations needs caution, but still our reading of their table 1 is that the significant amount of SN heating (i.e., their $\epsilon > 1$) is required to simultaneously account for the L_X – T relation and the hot gas fraction of ICM. This is consistent with our above successful parameter set $(\epsilon_{\text{SN}}, \epsilon_{\text{RG}}) = (3.0, 0.0)$ as we show below.

7. Statistical properties of simulated clusters

The metallicity-temperature relations of our simulated clusters in the six models are plotted in figure 5. We adopt equation (36) for f_{rh} even in the case of $\epsilon_{\text{RG}} \neq 0$ (right panels). Since the values of f_{rh} are chosen so as to reproduce the $Z - T_{\text{gas}}$ relation for $\epsilon_{\text{RG}} = 0$, the agreement in left panels is just by construction. Right panels in figure 5 confirm that the non-vanishing ϵ_{RG} does not affect the mean relation as mentioned in §5, but mainly add scatters around the mean due to the stochastic nature of heating by radio galaxies in our model. Note, however, that it is probably premature to compare the dispersions around the mean even if tempting. It is not clear to what extent the observational data reflect the intrinsic scatter rather than merely the observational errors. Furthermore our modeling is very simplified and ignores various possible sources for the dispersions; we assumed constant η_{SN} , f_{rh} , ϵ_{SN} , ϵ_{RG} , and so on which are likely to be dependent on the environment. In this sense, we expect that our model predictions systematically underestimate the real scatters. This remark should apply also to the other statistical properties discussed in this section.

Figure 6 shows the degree of the goodness-of-fit of the luminosity–temperature relation in detail for the six sets of model parameters. Top panels indicate that the supernova feedback is indeed essential in explaining the L_{bol} – T relation. Middle and bottom panels suggest that the jet heating is relatively insignificant if efficiency of the supernova feedback is high. Although the $\tilde{\chi}_{\text{red}}^2$ -statistics in figure 4 may indicate a marginally acceptable fit in the case of $(\epsilon_{\text{SN}}, \epsilon_{\text{RG}}) = (1.0, 0.0)$, further heating (either by the jet or by much higher star formation efficiency as

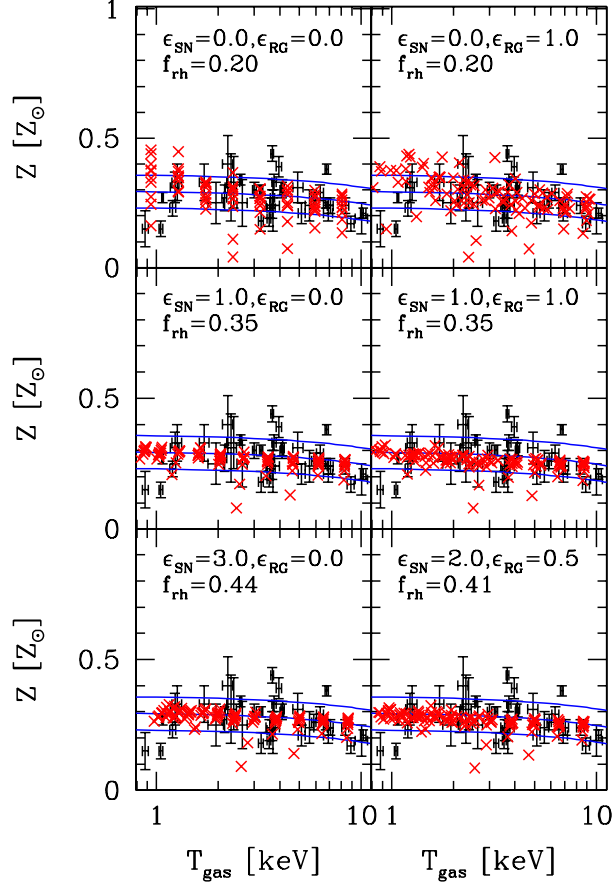


Fig. 5. Scatter plots of the metallicity-temperature relation of clusters at $z = 0$. Our model predictions are plotted in crosses, and the observed Fe abundances (Fukazawa et al. 1998) are plotted in dots with error-bars. The solid lines indicate the mean observational metallicity-temperature relation and the corresponding $\pm 1\sigma$ dispersions.

empirically proposed in §8 below) is indeed preferred. It is interesting to note that the jet heating sometimes produces an *X-ray dark cluster*. This corresponds to a cluster in the middle-right panel of figure 6; the mass and the temperature of the cluster is $7.9 \times 10^{13} M_{\odot}$, and 2.7 keV while it is very X-ray faint ($L_{\text{bol}} \sim 7 \times 10^{42} \text{ erg s}^{-1}$). This is an illustrative example which reflects the stochastic nature of the jet heating.

Figure 7 shows the results for the mass – temperature relation of the clusters, which are in good agreement with the conclusions in figure 6; we need strong heating sources to match the observed $M - T$ relation (Finoguenov et al. 2001). While this may be due to the fact that the $M - T$ relation is not entirely independent of the $L_{\text{bol}} - T$ relation (since our current model adopts the specific density and temperature profiles as a function of mass alone), it will provide additional insight at least (see also Shimizu et al. 2003).

The successful heating models also reproduce well the observed hot gas fraction of clusters. In figure 8, we plot the hot gas mass fraction in halos at $z = 0$ against their gas temperature, $f_{\text{hot}}(T_{\text{gas}}) \equiv M_{\text{hot}}/(\Omega_{\text{B}} M_{\text{halo}}(T_{\text{gas}})/\Omega_{\text{M}})$. Again the average value of $f_{\text{hot}}(T_{\text{gas}})$ is mainly

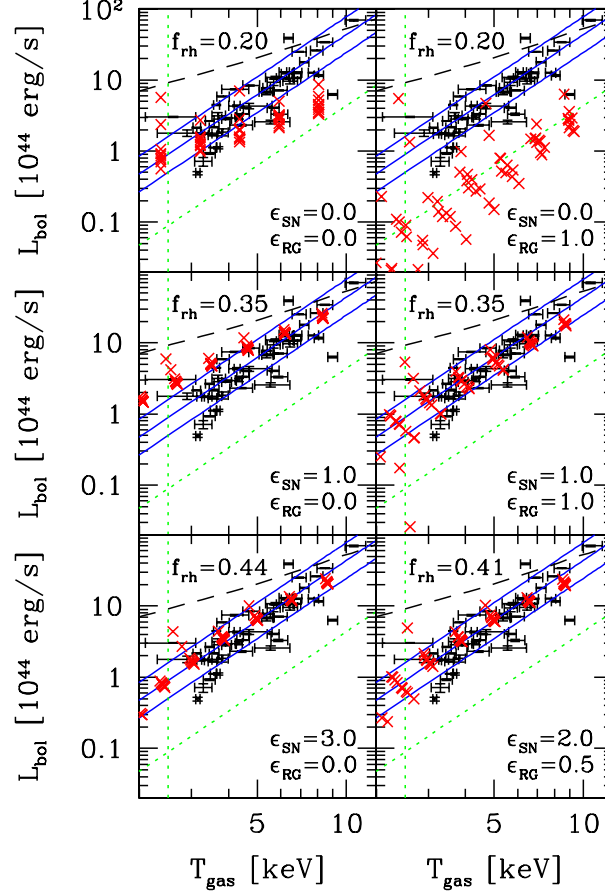


Fig. 6. Scatter plots of the luminosity-temperature relation of clusters at $z = 0$. Our model predictions are plotted in crosses, and the observational data (Ikebe et al. 2002) are plotted in dots with error-bars. The solid lines indicate the mean observational luminosity-temperature relation and the corresponding $\pm 1\sigma$ dispersions. The dotted lines represent our selection criteria; $T_{\text{gas}} > 2.5$ keV and 0.1 times the mean $L_{\text{bol}}(T_{\text{gas}})$. The dashed line indicates the ‘self-similar’ relation corresponding to figure 3.

controlled by the amount of supernova energy feedback, and is fairly insensitive to the value of ϵ_{RG} . Note that cooling of ICM is so efficient and without non-gravitational heating most of the ICM remains cold. This is another reason why a significant amount of non-gravitational heating is required in galaxy clusters (again not entirely independent of the luminosity – temperature relation, though).

Ponman et al. (1999) find that the ‘core entropy’, S_c , of low temperature clusters ($T_{\text{gas}} \sim 1$ keV) is much larger than the self-similar model prediction, where $S_c = k_B T_{\text{gas}} / [n_e(r_c)]^{2/3}$ is defined at the core radius r_c . This departure from the self-similarity of ICM also supports the importance of non-gravitational heating/cooling processes in the evolution of galaxy clusters; when some fraction of gas in the ICM cools, the hot gas density responsible for the entropy is reduced and the gas entropy increases. Of course the gas entropy is increased by the temperature rise and the resulting spreading of the core region due to non-gravitational heating. In reality, both processes are intimately coupled with each other and one has to trace the thermal evolution

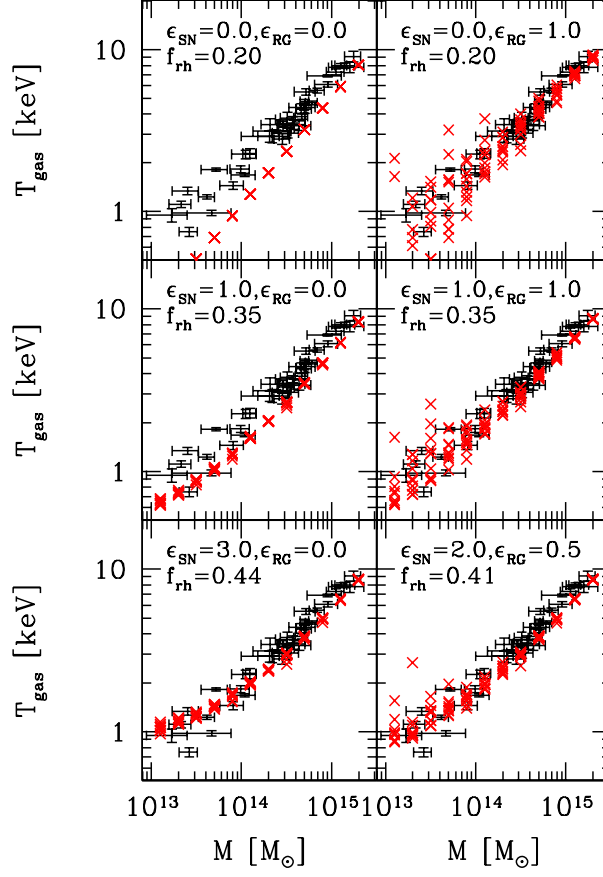


Fig. 7. Scatter plots of the mass-temperature relation of clusters at $z = 0$. Our model predictions are plotted in crosses. The dots with vertical and horizontal error-bars indicate the observational data points of Finoguenov et al. (2001) after appropriate correction for the virial mass (c.f., Appendix A in Shimizu et al. 2003).

of ICM taking account of heating and cooling in a self-consistent fashion. Although this seems a straightforward project for hydrodynamic numerical simulations, it is not easy to reliably trace the thermal evolution over the required dynamic range between $\lesssim 10^7 M_\odot$ (that can cool at $z \sim 30$ corresponding to the virial temperature of $\sim 10^4 \text{K}$) and $\gtrsim 10^{16} M_\odot$ (that encloses the region surrounding a rich cluster) given the limited mass resolution of current simulations. This is exactly why our current approach plays a complementary role in studying the thermal evolution of ICM.

Figure 9 shows the core ‘entropy’ against the gas temperature of halos at $z = 0$. In the plot, we adopt a simple definition for the core radius, $r_c = 0.1 r_{\text{vir}}$, which is approximately consistent with most observed clusters. We estimate $n_e(r)$ from equation (17) assuming that the hot gas is in collisional ionization equilibrium. Despite such crude definitions adopted tentatively, our heating models fairly reproduce the observational best fit relation by Ponman et al. (2003) and the value of the entropy ‘floor’ by Lloyd-Davies et al. (2000).

Finally the excess energy per gas particle, ΔE_{gas} , is plotted in figure 10 against the

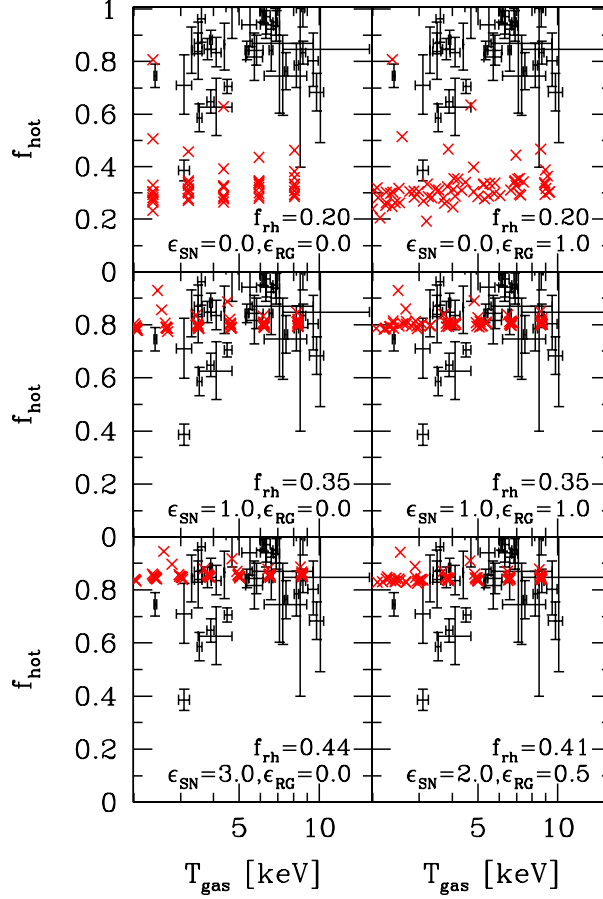


Fig. 8. Scatter plots of the hot gas fraction of clusters $z = 0$. Our model predictions are plotted in crosses. The observational data points are taken from Mohr et al. (1999), but are multiplied by Ω_M/Ω_B .

halo mass at $z = 0$. As expected, all the successful models (middle and bottom panels) have $\Delta E_{\text{gas}} \sim 1 \text{ keV/particle}$. As we have seen in other plots, the jet from radio galaxies increases the dispersion. Note that the excess energy is defined as per one hot gas particle; the hot gas mass fraction in the top-right panel is merely 30 percent and this is why ΔE_{gas} ranges up to $\sim 2 \text{ keV/particle}$ although the total heating energy is less than the other models (middle and bottom panels).

As we mentioned in Introduction, our current approach corresponds to the improved modeling of the earlier work by Wu et al. (2000). Thus it is relevant to compare the results here. They concluded that the excess energy of $\sim (1-3) \text{ keV/particle}$ is required to reproduce the observed luminosity – temperature relation. This is in good agreement with others as well as our results (figure 10). They also argued that this amount of excess energy is unlikely to be provided by supernova feedback except in a highly contrived model of galaxy formation, and suggested the AGNs as a potentially important heating source. In this respect, the normalization of our model parameter, ϵ_{SN} , may be a bit optimistic; they assume the average kinetic energy from supernova of $4 \times 10^{50} \epsilon_{\text{Wu,SN}} \text{ erg}$ with their efficiency parameter $\epsilon_{\text{Wu,SN}} \sim 0.3$, while we adopted

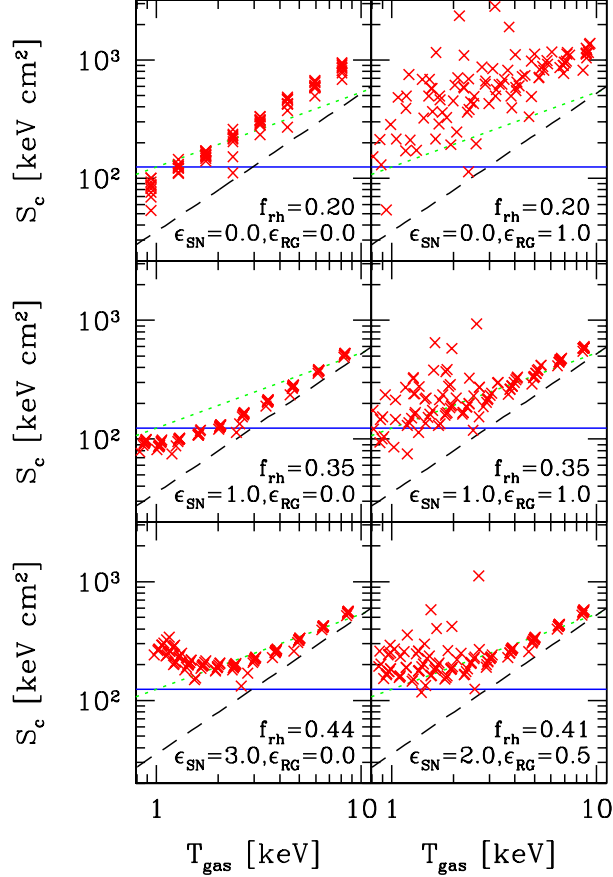


Fig. 9. Scatter plots of the core ‘entropy’ of clusters at $z = 0$. Our model predictions are plotted in crosses. The solid line indicates the entropy floor of $124 h_{70}^{-1/3} \text{ keV cm}^2$ from Lloyd-Davies et al. (2000). The dotted line is the observational best-fit relation by Ponman et al. (2003). The dashed line represents the self-similar model prediction.

$10^{51} \epsilon_{\text{SN}} \text{ erg}$. Since they did not show plots of the statistical properties of their resulting clusters as we did in the present section, further quantitative comparison is difficult, but the above overall qualitative conclusions seem to be in reasonable agreement with each other.

8. Model of higher star formation activities at $z > 7$

One reasonable interpretation of the recent *WMAP* result on the early reionization at $z = 17 \pm 5$ (Spergel et al. 2003) is that the star formation rate was much higher and/or the energy injection from supernovae was stronger; it has been argued that the first objects at high redshifts may be preferentially very massive ($\sim 100 M_{\odot}$), and that their birth rate may be higher than those in the range $1\text{--}2 M_{\odot}$ (e.g., Bromm et al. 1999; Abel et al. 2000; Nakamura, Umemura 2001). Such first objects may turn into hypernovae with the explosion energy $\gtrsim 10^{52} \text{ erg}$. In order to mimic such *plausible* scenarios, we consider a model with the bimodal supernova feedback efficiency:

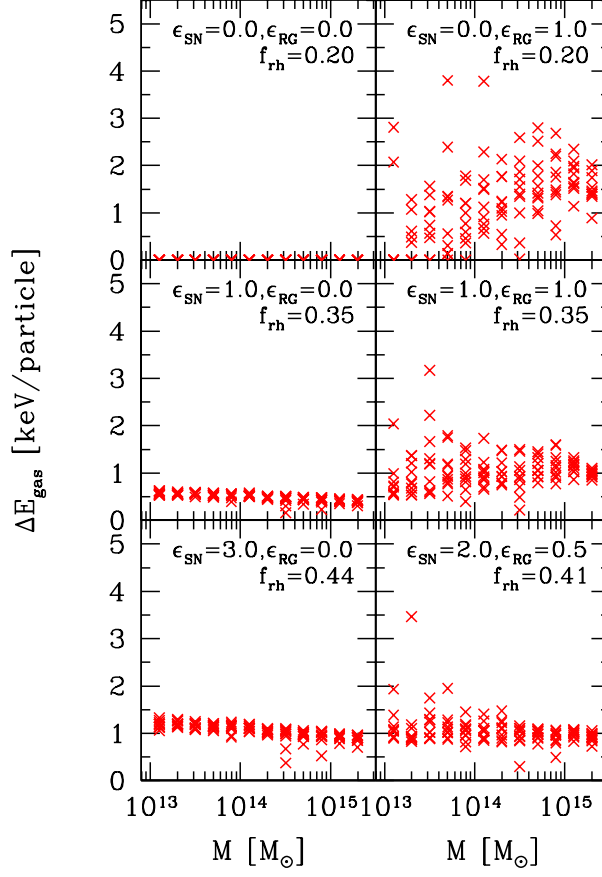


Fig. 10. Scatter plots of the excess energy per gas particle of clusters at $z = 0$. Our model predictions are plotted in crosses.

$$\epsilon_{\text{SN}} = \begin{cases} \epsilon_{\text{SN,L}} & (z < 7) \\ \epsilon_{\text{SN,H}} & (z \geq 7) \end{cases}. \quad (40)$$

For definiteness we fix that $\epsilon_{\text{SN,L}} = 0.3$, corresponding to the 30 percent conversion efficiency of the supernova energy to the ICM thermalization. Since the efficiency at high z is much more uncertain, we explore the four cases; $\epsilon_{\text{SN,H}} = 1.0, 2.0, 5.0$, and 10.0 . We neglect the jet heating, i.e., $\epsilon_{\text{RG}} = 0$, and adopt that $f_{\text{rh}} = 0.26$ [equation (36) with $\epsilon_{\text{SN}} = 0.3$] at all redshifts.

Figure 11 shows that the luminosity-temperature relation of the model clusters for $\epsilon_{\text{SN,H}} \sim 5.0$ (lower left panel) reproduces the observation reasonably well. This may correspond to an original idea of *preheating* by Evrard, Henry (1991) and Kaiser (1991), and thus the result is fairly insensitive to non-gravitational heating at lower redshifts.

The other relations are shown in figure 12 for $\epsilon_{\text{SN,L}} = 0.3$ and $\epsilon_{\text{SN,H}} = 5.0$. Since we did not attempt to tune the parameter sets, we would say that the agreement is satisfactory; the inclusion of the jet heating by radio galaxies at low redshifts would certainly improve the agreement. These results are impressive because we do not have to consider exceedingly strong supernova feedback at low redshifts if the star formation activity at high redshifts is sufficiently enhanced.

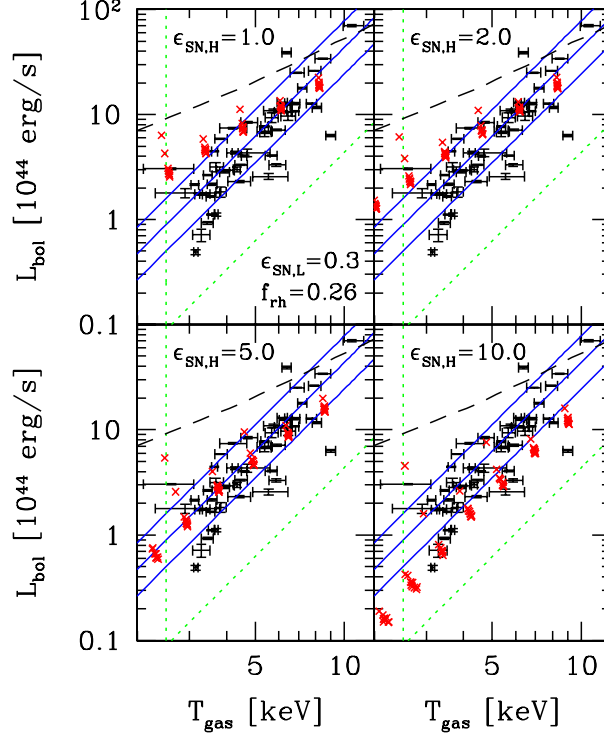


Fig. 11. Same as figure 6 but for models with enhanced star formation activity for $z > 7$. We assume that $\epsilon_{\text{RG}} = 0$ and $f_{\text{rh}} = 0.26$ at all redshifts.

9. Summary and conclusions

We have developed a semi-analytical approach to trace the thermal history of galaxy clusters based on the Monte-Carlo modeling of merging trees of dark matter halos. Under the assumption of hydrostatic equilibrium and the isothermal gas profiles, we have incorporated the metallicity evolution, the metallicity-dependent cooling of gas, the supernova energy feedback, and heating due to the jet of radio galaxies in a consistent manner. The latter non-gravitational heating processes were characterized by two dimensionless parameters, ϵ_{SN} and ϵ_{RG} , and we explored several statistical properties of galaxy clusters over a wide range of the parameter space.

As has been known for a while, we confirmed that a fiducial model of supernova feedback alone, i.e., $\epsilon_{\text{SN}} < 1$, does not reproduce the observed luminosity – temperature relation of clusters. A reasonable agreement can be achieved by enhancing non-gravitational heating in two different ways; i) considering additional heating due to the jet of some class of AGNs, notably Type II of the Fanaroff-Riley radio galaxies, and ii) adopting somewhat higher star formation efficiency and/or supernova energy feedback. The former possibility was first examined seriously by Inoue, Sasaki (2001), and the current study basically confirmed their conclusion using a significantly improved methodology to trace the thermal history of ICM. The latter idea is particularly interesting in the light of the recent *WMAP* finding of the earlier reionization epoch of the

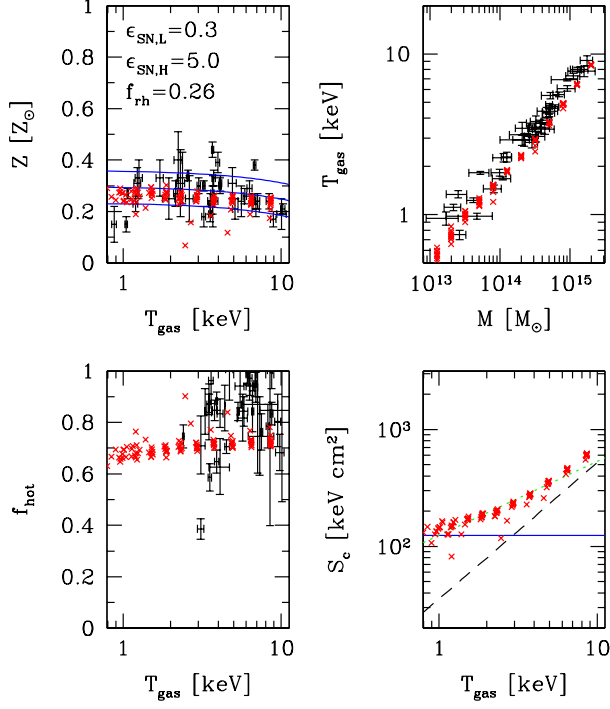


Fig. 12. Scatter plots of the metallicity-temperature relation, the mass-temperature relation, the hot gas fraction, and the core ‘entropy’ for models with enhanced star formation activity for $z > 7$. Our model predictions are plotted in crosses. We assume that $\epsilon_{\text{SN,L}} = 0.3$ and $\epsilon_{\text{SN,H}} = 5.0$, while the other parameters have the same values as in figure 11.

universe than previously thought. By increasing the feedback efficiency at high redshifts ($\epsilon_{\text{SN}} \sim 5$ at $z > 7$, for instance), most of the model predictions of the simulated clusters can be brought into agreement with the observational data.

So far we discussed several properties of clusters at $z = 0$, and did not examine their evolution. Considering the success of the enhanced star formation activity model, it is important to combine the ICM heating model with the cosmic star formation history. In doing that, we will have tighter constraints on the parameter space of ϵ_{SN} and ϵ_{RG} , and may have a link to the physical reasonable scenario beyond a general but parameterized modeling like our current approach. A future sample of clusters at high z selected by the Sunyaev-Zel’dovich effect (Sunyaev, Zel’dovich 1972) may provide another complementary piece of information on the thermal evolution of the ICM. We hope to report results on these important issues elsewhere in due course.

This research was supported in part by the Grant-in-Aid for Scientific Research of JSPS (12640231, 14102004, 14740133, 15740157). Numerical computation was performed using computer facilities at the University of Tokyo supported by the Special Coordination Fund for Promoting Science and Technology, Ministry of Education, Culture, Sport, Science and Technology.

Appendix. Tracing thermal evolution of ICM in merging trees of dark matter halos

In the present paper, we trace merger trees from $z = 0$ to $z = 30$. In this case, however, the number of progenitors in one merging tree becomes progressively larger at higher redshifts, and it is not practically feasible. Thus we decide to prepare two different sets of merger trees at low redshifts ($z = 0$ to $z = 7$) and at high redshifts ($z = 7$ to $z = 30$).

We first construct $N_{\text{ens}} (=10)$ independent sets of merger tree realizations for each value of 12 different masses of M_{root} starting from $z_{\text{min}} = 0$ to $z_{\text{max}} = 7$ in $N_{\text{step}} = 750$ timesteps. We also construct separately 20 sets of merger tree realizations starting from $z_{\text{min}} = 7$ to $z_{\text{max}} = 30$ in $N_{\text{step}} = 500$ timesteps. We use the number of timesteps in logarithmically equal redshift interval, $N_{\text{step}} = 750$ for the low z sets and $N_{\text{step}} = 500$ for the high z sets. The masses of the root halo M_{root} are equal to $10^{13+0.2(i-0.5)} M_{\odot}$ ($i = 1, \dots, 12$) at $z = 0$ for the low z sets, and $2.0 \times 10^{7+j} M_{\odot}$ ($j = 1, \dots, 6$) at $z = 7$ for the high z sets. The minimal mass of progenitors resolved in the merger tree M_{res} is equal to $M(T_{\text{vir}} = 10^4 \text{ K})$, which corresponds to a mass of halos whose virial temperature is 10^4 K at each redshift. The parameters concerning the merging tree of halos is summarized in table 3.

Table 3. Parameters for merger trees of dark halos.

symbol	adopted value		physical meaning
	low redshift	high redshift	
M_{root}	$10^{13+0.2(i-0.5)} M_{\odot}$ ($i = 1, \dots, 12$)	$2.0 \times 10^{7+j} M_{\odot}$ ($j = 1, \dots, 6$)	mass of halo at $z = z_{\text{min}}$
M_{res}	$M(T_{\text{vir}} = 10^4 \text{ K})$		minimal mass of progenitors resolved in each merger tree
N_{step}	750	500	number of redshift bins (logarithmically equal interval)
N_{ens}	10	20	number of realizations of the merger tree
z_{min}	0	7	minimum redshift of the merger tree
z_{max}	7	30	maximum redshift of the merger tree

Assuming that baryons at $z = 30$ have their gas temperature equal to the virial temperature of their individual host halo, both the halo merging history and the thermal evolution of gas are followed up to $z = 7$. At that redshift, each halo is assigned to another realization of the halo in the separate redshift merger trees using the interpolation of the mass in finding its counterpart. Then all the properties of the halo at high redshift tree is now transferred to its counterpart at the low redshift trees. Then we continue to follow its evolution until $z = 0$ tracing the new merging tree.

We checked the validity of the above interpolation method explicitly by constructing the merger trees from $z = 0$ to $z = 10$, and tracing the evolution using each merger tree. The

comparison with the results based on statistically connecting two separate merger trees from $z = 0$ to $z = 7$ and from $z = 7$ to $z = 10$ indicates that the properties of clusters at $z = 0$ are almost indistinguishable.

References

- Abel, T., Bryan, G. L., & Norman, M. L. 2000, *ApJ*, 540, 39
- Arnaud, M., & Evrard, E. 1999, *MNRAS*, 305, 631
- Balogh, M. L., Babul, A., & Patton, D. R. 1999, *MNRAS*, 307, 463
- Bicknell, G. V. 1995, *ApJS*, 101, 29
- Blundell, K. M., & Rawlings, S. 2000, *AJ*, 119, 1111
- Bond, J., Cole, S., Efstathiou, G., & Kaiser, N. 1991, *ApJ*, 379, 440
- Bower, R. 1991, *MNRAS*, 248, 332
- Bower, R. G., Benson, A. J., Lacey, C. G., Baugh, C. M., Cole, S., & Frenk, C. S. 2001, *MNRAS*, 325, 497
- Brighenti, F., & Mathews, W. G. 2002, *ApJ*, 553, 103
- Bromm, V., Coppi, P. S., & Larson, R. B. 1999, *ApJ*, 527, 5
- Buote, D. A. 2002, *ApJL*, 574, 135
- Bullock, J. S., Kolatt, T. S., Sigad, Y., Somerville, R. S., Kravtsov, A. V., Klypin, A. A., Primack, J. R., & Dekel, A. 2001, *MNRAS*, 321, 559
- Cavaliere, A., Menci, N., & Tozzi, P. 1999, *MNRAS*, 308, 599
- David, L. P., Forman, W., & Jones, C. 1990, *ApJ*, 359, 29
- David, L. P., Forman, W., & Jones, C. 1991a, *ApJ*, 369, 121
- David, L. P., Forman, W., & Jones, C. 1991b, *ApJ*, 380, 39
- David, L. P., Slyz, A., Jones, C., Forman, W., Vrtillek, S. D., & Arnaud, K. A. 1993, *ApJ*, 367, 45
- Elbaz, D., Arnaud, M., & Vangioni-Flam, E. 1995, *A&A*, 303, 345
- Enßlin, T. A., Biermann, P. L., Kronberg, P. P., & Wu, X. P. 1997, *ApJ*, 477, 560
- Enßlin, T. A., & Kaiser, C. R. 2000, *A&A*, 360, 417
- Evrard, A. E., & Henry, J. P. 1991, *ApJ*, 383, 95
- Fabian, A. C. 2001, in *ASP Conf. Ser. 250, Particles and Fields in Radio Galaxies Conference*, ed. R. A. Laing, & K. M. Blundell (San Francisco: ASP), 471
- Falle, S. A. E. G. 1991, *MNRAS*, 167, 31
- Finoguenov, A., Reiprich, T. H., & Böhringer, H. 2001, *A&A*, 368, 749
- Fukazawa, Y. et al. 1998, *PASJ*, 50, 187
- Hardcastle, M. J., & Worrall, D. M. 2000, *MNRAS*, 319, 562
- Ikebe, Y. et al. 1992, *ApJ*, 384, L5
- Ikebe, Y., Reiprich, T. H., Böhringer, H., Tanaka, Y., & Kitayama, T. 2002, *A&A*, 383, 773
- Inoue, S., & Sasaki, S. 2001, *ApJ*, 562, 618
- Kaiser, N. 1986, *MNRAS*, 222, 323
- Kaiser, N. 1991, *ApJ*, 383, 104
- Kay, S. T., Thomas, P. A., & Theuns, T. 2003, *MNRAS*, 343, 608
- Kauffmann, G., & White, S. D. M. 1993, *MNRAS*, 261, 921
- Kitayama, T., & Suto, Y. 1996, *ApJ*, 469, 480
- Kravtsov, A. V., & Yepes, G. 2000, *MNRAS*, 318, 227
- Kroupa, P. 2001, *MNRAS*, 322, 231
- Kroupa, P. 2002, *Science*, 295, 82

- Laing, R. A. 1996, in ASP Conf. Ser. 100, Energy Transport in Radio Galaxies and Quasars, ed. P. E. Hardee, A. H. Bridle, & J. A. Zensus (San Francisco: ASP), 241
- Leahy, J. P., & Gizani, N. A. B. 2001, *ApJ*, 555, 709
- Lloyd-Davies, E. J., Ponman, T. J., & Cannon, D. B. 2000, *MNRAS*, 315, 689
- Loewenstein, M. 2000, *ApJ*, 532, 17
- Markevitch, M. 1998, *ApJ*, 504, 27
- Mohr, J. J., Mathiesen, B., & Evrard, A. E. 1999, *ApJ*, 517, 627
- Muanwong, O., Thomas, P. A., Kay, S. T., & Pearce, F. R. 2002, *MNRAS*, 336, 527
- Nath, B. B., & Roychowdhury, S. 2002, *MNRAS*, 333, 145
- Nakamura, F., & Umemura, M. 2001, *ApJ*, 548, 19
- Navarro, J. F., Frenk, C. S., & White, S. D. M. 1996, *ApJ*, 462, 563
- Oguri, M., Taruya, A., & Suto, Y. 2001, *ApJ*, 559, 572
- Pen, U. 1999, *ApJL*, 510, 1
- Ponman, T. J., Cannon, D. B., & Navarro, J. F. 1999, *Nature*, 397, 135
- Ponman, T. J., Sanderson, A. J. R., & Finoguenov, A. 2003, *MNRAS*, 343, 331
- Rawlings, S. 1992, *Extragalactic Radio Sources: From Beams to Jets*, ed. J. Roland, H. Sol, & G. Pelletier (Cambridge: Cambridge Univ. Press), 332
- Sheth, R. K., & Lemson, G. 1999, *MNRAS*, 305, 946
- Shimizu, M., Kitayama, T., Sasaki, S., & Suto, Y. 2002, *PASJ*, 54, 645.
- Shimizu, M., Kitayama, T., Sasaki, S., & Suto, Y. 2003, *ApJ*, 590, 197.
- Somerville, R. S., & Kolatt, T. S. 1999, *MNRAS*, 305, 1
- Spergel, D. N. et al. 2003, *ApJS*, 148, 175
- Sunyaev, R. A., & Zel'dovich, Y. B. 1972, *Comm. Astrophys. Space Phys.*, 4, 173
- Sutherland, R. S., & Dopita, M. A. 1993, *ApJS*, 88, 253
- Suto, Y., Sasaki, S., & Makino, N. 1998, *ApJ*, 509, 544
- Tornatore, L., Borgani, S., Springel, V., Matteucci, F., Menci, N., & Murante, G. 2003, *MNRAS*, 342, 1025
- Valageas, P., & Silk, J. 1999, *A&A*, 350, 725
- Valdarnini, P. 2003, *MNRAS*, 339, 1117
- Voit, G. M., & Bryan, G. L. 2001, *Nature*, 414, 425
- Willott, C. J., Rawlings, S., Blundell, K. M., & Lacy, M. 1999, *MNRAS*, 309, 1017
- Willott, C. J., Rawlings, S., Blundell, K. M., Lacy, M., & Eales, S. A. 2001, *MNRAS*, 322, 536
- Wu, K. K. S., Fabian, A. C., & Nulsen, P. E. J. 2000, *MNRAS*, 318, 889
- Wu, X.-P., & Xue, Y.-J. 2002, *ApJL*, 572, 19